PETROLEUM EXPLORATION AND DEVELOPMENT
Volume 52, Issue 5, October 2025
http://www.sciencedirect.com/journal/petroleum-exploration-and-development

Available online at www.sciencedirect.com
ScienceDirect

Cite this article as: PETROL. EXPLOR. DEVELOP., 2025, 52(5): 1179–1192.

RESEARCH PAPER

Structural physical simulation experiment on vertical growth process of strike-slip faults in ultra-deep strata of Tarim Basin, NW China

NENG Yuan[1, *], XIE Zhou[2], SHAO Longfei[1], RUAN Qiqi[3], KANG Pengfei[2], ZHANG Jianan[1], TIAN Zhiwen[1], LIU Genji[1]

1. College of Geosciences, China University of Petroleum (Beijing), Beijing 102249, China;
2. Exploration and Development Research Institute, PetroChina Tarim Oilfield Company, Korla 841000, China;
3. School of Petroleum, China University of Petroleum (Beijing) at Karamay, Karamay 834000, China

Abstract: In the ultra-deep strata of the Tarim Basin, the vertical growth process of strike-slip faults remains unclear, and the vertical distribution of fractured-cavity carbonate reservoirs is complex. This paper investigates the vertical growth process of strike-slip faults through field outcrop observations in the Keping area, interpretation of seismic data from the Fuman Oilfield, Tarim Basim, NW China, and structural physical simulation experiments. The results are obtained mainly in four aspects. First, field outcrops and ultra-deep seismic profiles indicate a three-layer structure within the strike-slip fault, consisting of fault core, fracture zone and primary rock. The fault core can be classified into three parts vertically: fracture-cavity unit, fault clay and breccia zone. The distribution of fracture-cavity units demonstrates a distinct pattern of vertical stratification, owing to the structural characteristics and growth process of the slip-strike fault. Second, the ultra-deep seismic profiles show multiple fracture-cavity units in the strike-slip fault zone. These units can be classified into four types: top fractured, middle connected, deep terminated, and intra-layer fractured. Third, structural physical simulation experiments and ultra-deep seismic data interpretation reveal that the strike-slip faults have evolved vertically in three stages: segmental rupture, vertical growth, and connection and extension. The particle image velocimetry detection demonstrates that the initial fracture of the fault zone occurred at the top or bottom and then evolved into cavities gradually along with the fault growth, accompanied by the emergence of new fractures in the middle part of the strata, which subsequently connected with the deep and shallow cavities to form a complete fault zone. Fourth, the ultra-deep carbonate strata primarily develop three types of fractured-cavity reservoirs: flower-shaped fracture, large and deep fault and staggered overlap. The first two types are larger in size with better reservoir conditions, suggesting a significant exploration potential.

Key words: strike-slip fault; vertical growth; evolution process; structural physical simulation experiment; Ordovician fractured-cavity carbonate reservoir; ultra-deep; Tarim Basin; Fuman oilfield

Introduction

In recent years, large-scale strike-slip faults have been identified within the Paleozoic carbonate formations in the platform area of the Tarim Basin. The fractured-cavity reservoirs controlled by these faults have attracted extensive attention from geologists worldwide. In particular, the Fuman Oilfield in the Tarim Basin, NW China, represents a typical fault-controlled karst region and has become a critical exploration target for increasing reserves and production from carbonate reservoirs in the Tarim Basin [1–9]. Numerous studies indicate that this type of strike-slip faults is structurally characterized by multi-phase deformation superimposition, vertically stratified distribution, and planar segmented rupture. Specifically, the vertically stratified distribution is controlled by varying formation lithology and multiple tectonic movements; the planar segmentation is governed by the internal structure and growth & linkage process of

Received date: 17 Oct. 2024; **Revised date:** 28 Aug. 2025.
*** Corresponding author.** E-mail: nengyuan@cup.edu.cn
Foundation item: Supported by the National Natural Science Foundation of China (42362026); Key R&D Project of Xinjiang Uygur Autonomous Region (2024B01015).
https://doi.org/10.1016/S1876-3804(25)60634-3

the strike-slip faults; and the multi- phase deformation superimposition is constrained by changes in the regional tectonic stress field [2, 6, 10–18]. The structural styles of strike-slip faults are diverse and complex in both plan and cross-section.

Structural physical simulation experiment is a vital technique for studying the formation and evolution of strike-slip faults. By designing various experimental models, researchers have yielded significant insights. Through physical simulation experiments, Cloos and Naylor divided the planar evolution of strike-slip fault zone into approximately four stages [19–20]. Xiao employed computed tomography (CT) imaging technology in physical simulation experiments to reconstruct the evolutionary process of strike-slip fault zone [21]. His work revealed a "spiral-dragging" development pattern in en echelon structures and demonstrated that incipient strike-slip structures splay upward in cross-section, forming deformation zones with appreciable width. Previous studies have predominantly focused on the planar distribution and lateral segmentation of strike-slip faults, but inadequately dealt with the vertical evolution process of the fault zone and its coupling with fracture-cavity units. During strike-slip faulting, surrounding rocks undergo fracturing. Subsequent subaerial exposure and dissolution or the influence of deep fluids can lead to the formation of fault-controlled fractured-cavity reservoirs, which exhibit a distinctive "beaded" reflection pattern on seismic profiles [13, 22]. Exploration findings in the Fuman Oilfield demonstrate that fractured-cavity reservoirs associated with strike-slip faults distribute heterogeneously in vertical direction within the fault zone [6, 12, 14, 23–26]. The controlling effects of the complex internal structure and vertical growth processes of strike-slip faults on the distribution of fractured-cavity reservoirs remain poorly constrained and urgently require further research.

This study integrates detailed analysis of typical field outcrops, seismic profile interpretation, physical simulation experiment, and particle image velocimetry (PIV) monitoring to reconstruct the vertical evolution process of strike-slip faults, establish a structural model of strike-slip fault zone, and clarify the distribution patterns of fracture-cavity units within the fault zone. The study results provide a guidance for the exploration and development of ultra-deep fractured-cavity reservoirs in the Tarim Basin.

1. Regional geological setting

The Fuman Oilfield lies in the eastern part of the Aman Transitional Zone, within the platform area of the Tarim Basin (Fig. 1a). It is characterized by numerous NE–NNE-trending strike-slip faults, some of which exhibit significant activity, extending from the Tabei Uplift to the Central Uplift (Fig. 1b). The strata are complete and can be vertically divided into five major structural sequences: the pre-Nanhua basement, the Nanhua–Sinian rift basin, the Cambrian–Ordovician marine carbonate platform, the Silurian–Cretaceous marine-to-terrestrial transitional basin and the Cenozoic foreland basin. The Lower Paleozoic Cambrian–Ordovician marine carbonate formations in the Fuman Oilfield host significant hydrocarbon resources [5]. From bottom to top, the Cambrian System comprises the Yurtus, Xiaoerblak, Wusonggeer, Shayilik, Awatag and Lower Qiulitage formations, and the Ordovician System consists of the Penglaiba, Yingshan, Yijianfang, Tumuxiuke, Lianglitage and Sangtamu formations (Fig. 1c). The Lower Ordovician is in unconformable contact with the Upper Cambrian. The Penglaiba Formation (O_1p) is characterized by interbedded fine-crystalline dolomite and dolomitic micritic limestone. The Lower Yingshan Formation ($O_{1-2}y_1$), mainly $O_{1-2}y_1^{3-4}$, comprises thick-bedded argillaceous limestone with intercalations of dolomitic limestone. The Middle Ordovician features thick-bedded bioclastic and arenaceous limestones of shoal facies. In the Upper Ordovician, the Tumuxiuke and Lianglitage formations consist of thin-bedded calcareous mudstone and argillaceous limestone, respectively, while the Sangtamu Formation is composed of thick-bedded mudstone.

Hydrocarbon exploration mainly targets the carbonate rock formation of the Ordovician Yijianfang Formation (O_2y) and Upper Yingshan Formation ($O_{1-2}y_2$, mainly $O_{1-2}y_2^{1-2}$). With burial depths exceeding 7 000 m, these formations primarily develop fractured-cavity reservoirs due to the combined effects of strike-slip fault deformation, fragmentation and karstification processes [6]. The Lower Cambrian Yurtus Formation ($\in_1y$) contains effective source rocks, which charge the Ordovician reservoirs through strike-slip faults. The Upper Ordovician Sangtamu Formation (O_3s) provides a regionally extensive thick mudstone seal. Together, these elements form an excellent source-reservoir-seal assemblage [7].

2. Patterns of ultra-deep strike-slip fault zones

2.1. Structural characteristics of strike-slip fault in outcrops

According to outcrops in the Aoyipike section of the Tarim Basin, strike-slip fault zones exhibit complex structural characteristics within the Cambrian carbonate formations. The field outcrops are observed with characteristics as follows: (1) Four strike-slip faults (F1–F4) are identified (Fig. 2). F1 and F4 are major strike-slip faults. Ten secondary faults (f1–f10) are developed in the fault block between the two major faults. From the center to the branches, a strike-slip fault zone typically corresponds to a three-zone structure consisting of fault core, fractured zone and primary rock. The fault core is the most deformed portion of the strike-slip fault, where fracturing of primary rock leads to the development of

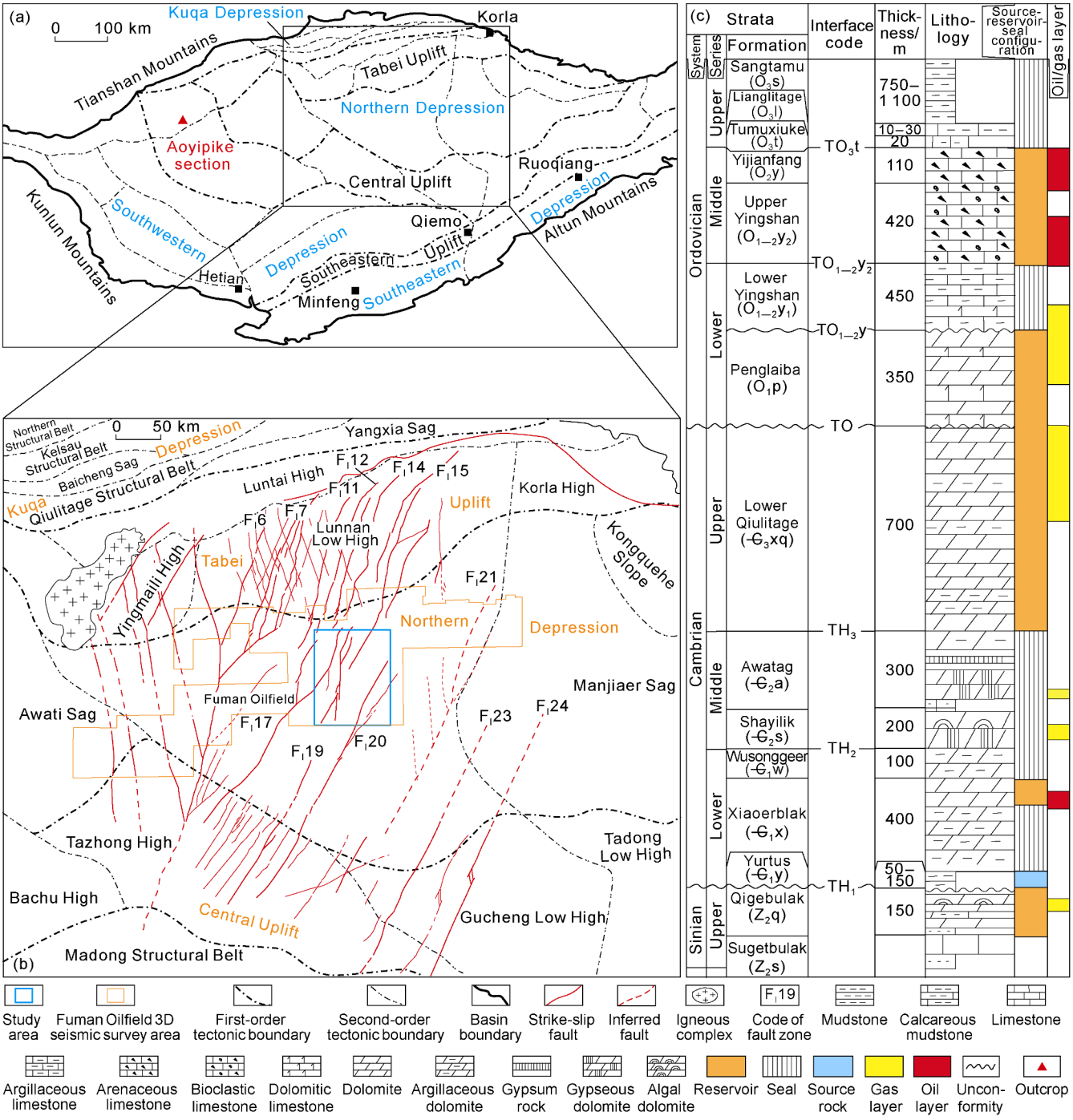

Fig. 1. Structural units of the Tarim Basin (a), location of the study area in the Fuman Oilfield (b), and comprehensive stratigraphic column (c) (modified according to Reference [7]). TH_1—Bottom of Yurtus Formation; TH_2—Bottom of Shayilik Formation; TH_3—Bottom of Lower Qiulitage Formation; TO—Bottom of Penglaiba Formation; $TO_{1–2}y$—Bottom of Lower Yingshan Formation; $TO_{1–2}y_2$—Bottom of Upper Yingshan Formation; TO_3t—Bottom of Tumuxiuke Formation.

cavities. The fractured zone is primarily influenced by strike-slip fault activity, resulting in intense fracturing of primary rock to generate a multitude of minor faults and joints (Fig. 2b). (2) The distribution of caivities (or fracture-caivity units) within the fault core is governed by the activity of the strike-slip fault, the geometry of the fault array, and the geometric relationship between the fault and the strata. F1, F2, and F3 exhibit higher activity than F4. Consequently, the scale of cavities and fractured formations within the fault zone on the right side is significantly larger than that on the left side. F2 and F3 are located in the hanging wall of F1, forming a flower-shaped structure that controls the distribution of cavities. Cavities form proximal to F1 within the fault block between F1 and F2, while cavities are most extensive near F3 within the block between F2 and F3. However, cavities along F1 are filled with collapsed fault blocks, resulting in an upward diminishment in cavity scale. At the junction of F1 and F3, the highest degree of rock fragmentation is observed. F4 has no secondary faults, and generally

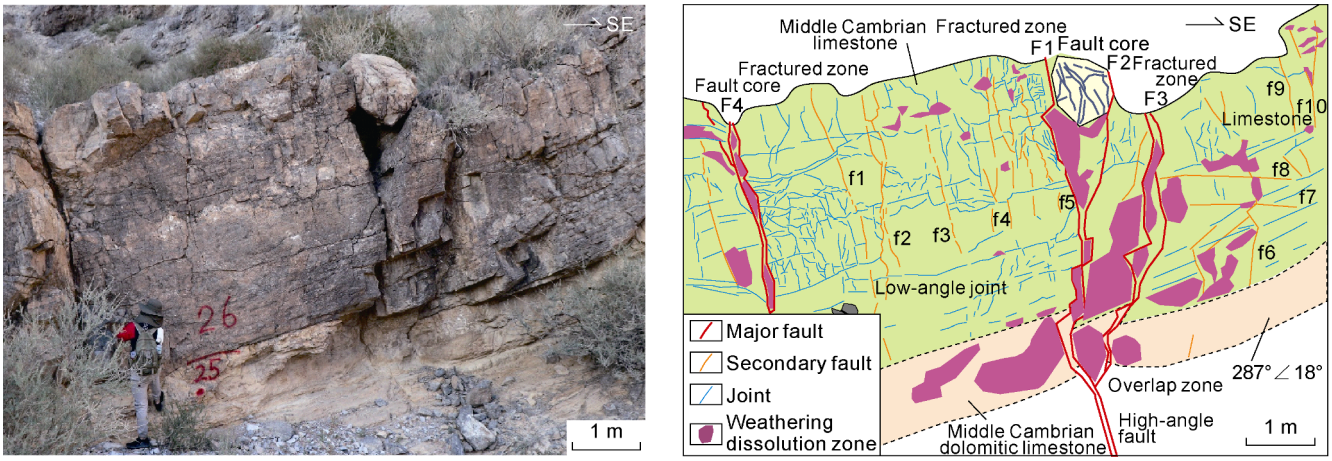

(a) Photograph of the field outcrop section

(b) Interpreted geological section

Fig. 2. Vertical structures of the strike-slip fault zone in the Aoyipike section, Tarim Basin (see the section location in Fig. 1a).

contains poorly developed cavities within its core, with their scale being significantly larger in both the upper and lower parts of the strata than in the middle part. As shown in Fig. 2a, a lithological difference exists between Bed 25 and Bed 26, with the underlying dolomitic limestone exhibiting higher dolomite content. This contrast resulted in pronounced bed-parallel fracturing along the formation interface. These faults are collectively controlled by the strike-slip fault and the stratigraphic boundary, with the most intense fracturing occurring at their intersection. (3) In addition to the fault core, abundant joints are developed within the fractured zone. The area between F1 and F4 exhibits the most intense joint development, primarily consisting of three sets of joints that are perpendicular, parallel, and oblique to the stratigraphic boundary, respectively. Fault cavities are poorly developed within the fractured zone, but only small-scale cavities occur proximal to the top of the strata and lithological interfaces.

Despite their reduced scale, outcrop-scale faults reveal heterogeneous rupture patterns and structures that are essential for seismic interpreters to develop a geological model for interpreting ultra-deep seismic data.

2.2. Vertical characteristics of strike-slip faults and fracture-cavity units in 3D seismic profiles

The Fuman Oilfield is a major target for fault-controlled fractured-cavity reservoir development in the Tarim Basin. Among its structures, the F_I19 fault zone serves as a key option for current reserve and production enhancement. This zone is sandwiched between the NE-striking F_I17 and F_I20 fault zones (Fig. 1b), yet exhibits distinct structural characteristics compared to the surrounding large-scale NE-trending strike-slip fault systems. It demonstrates more complex patterns of planar segmentation and better developed overlap zones. The N-S striking strike-slip fault in the middle part of the F_I19 fault zone cuts the NE-striking strike-slip faults in the southern and northern parts. This structural relationship is representative within the strike-slip fault system of the Aman Transitional Zone in the Tarim Basin [2].

According to 3D seismic data across the F_I19 fault zone in the Tarim Basin, seismic profiles reveal multiple types of "beaded" reflection patterns, which are distributed within different strata and generally exhibit the characteristics in three aspects. First, beaded reflections are pronounced near the major faults. The more active the major fault, the more complex the structural style observed in the seismic profile. Profiles through wells T4 and Y3 (Fig. 3) reveal that the largest beads exist within the fault core of the flower-shaped structure inside the strike-slip fault zone. On the profile across Well Y3, the beads are most developed at the intersection between the strike-slip fault and the top of the Ordovician carbonate formation (TO_3t), as shown in Fig. 3c. In contrast, on the western side of the F_I19 fault zone, the seismic profile displays vertically oriented faulting with no significant fracture-cavity development. The section across Well Y5 (Fig. 3d) exhibits a laterally-linked fault zone where the most extensive beaded reflections occur, indicating that the structural style of the strike-slip fault in profile view exerts a primary control on the development location of fracture-cavity units. Second, the distribution of beaded reflections exhibits notable variations across different formations within the fault zone. On the western side of the profile across Well Y3, these reflections are present in both deep and shallow parts of the Middle–Lower Ordovician carbonate formations (Fig. 3c), displaying vertically staggered overlap patterns. For faults on the eastern side, beads are revealed in the Upper Yingshan Formation and the Lower Yingshan Formation, and the deep beads are not interconnected with shallow ones, with the former larger in scale. Third, beaded reflections are not only controlled by the main strike-slip faults, a series of intraformational beaded reflections also occur within the Penglaiba Formation. The beaded reflections are not only

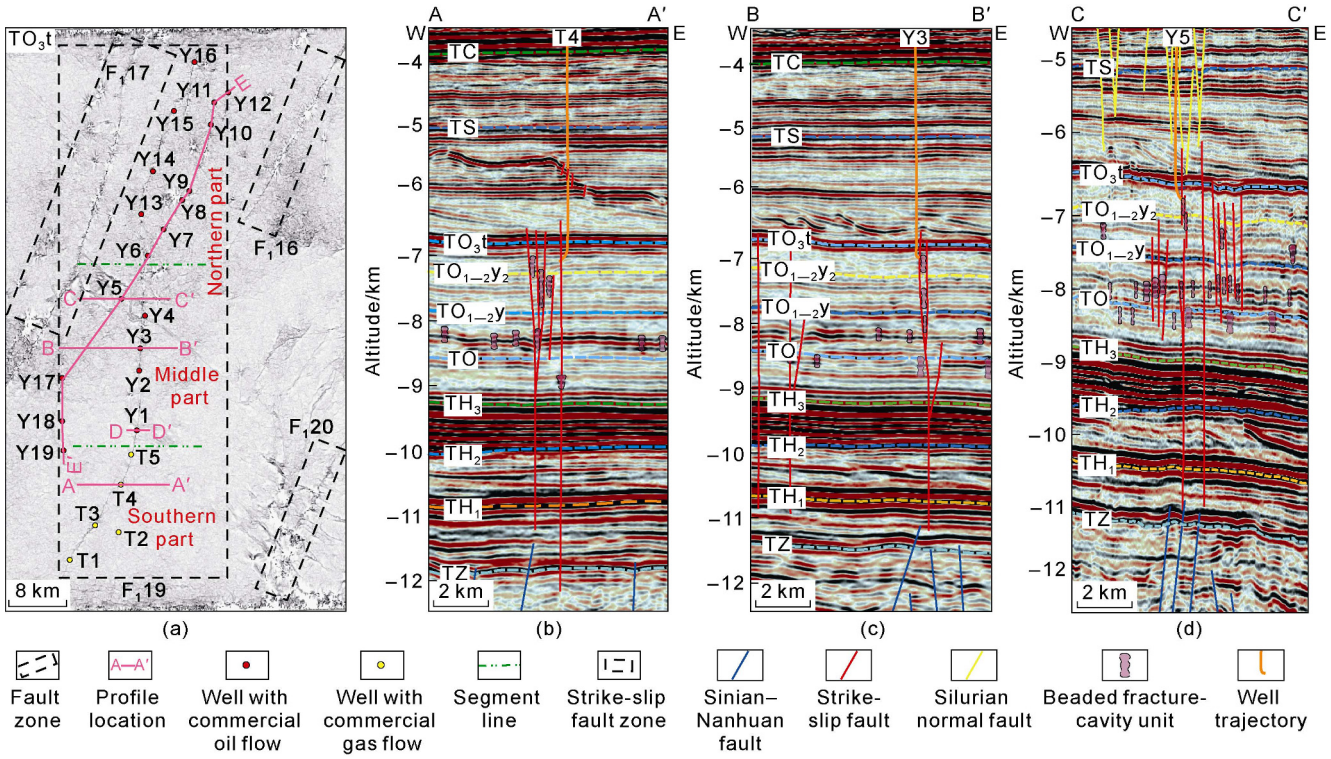

Fig. 3. Planar distribution of major faults at the top of Yijianfang Formation in the Fuman Oilfield (a) and representative seismic profiles across the $F_1$19 fault zone (b)–(d). TZ—bottom of Sinian Sugetbulak Formation; TS—bottom of Silurian; TC—bottom of Carboniferous.

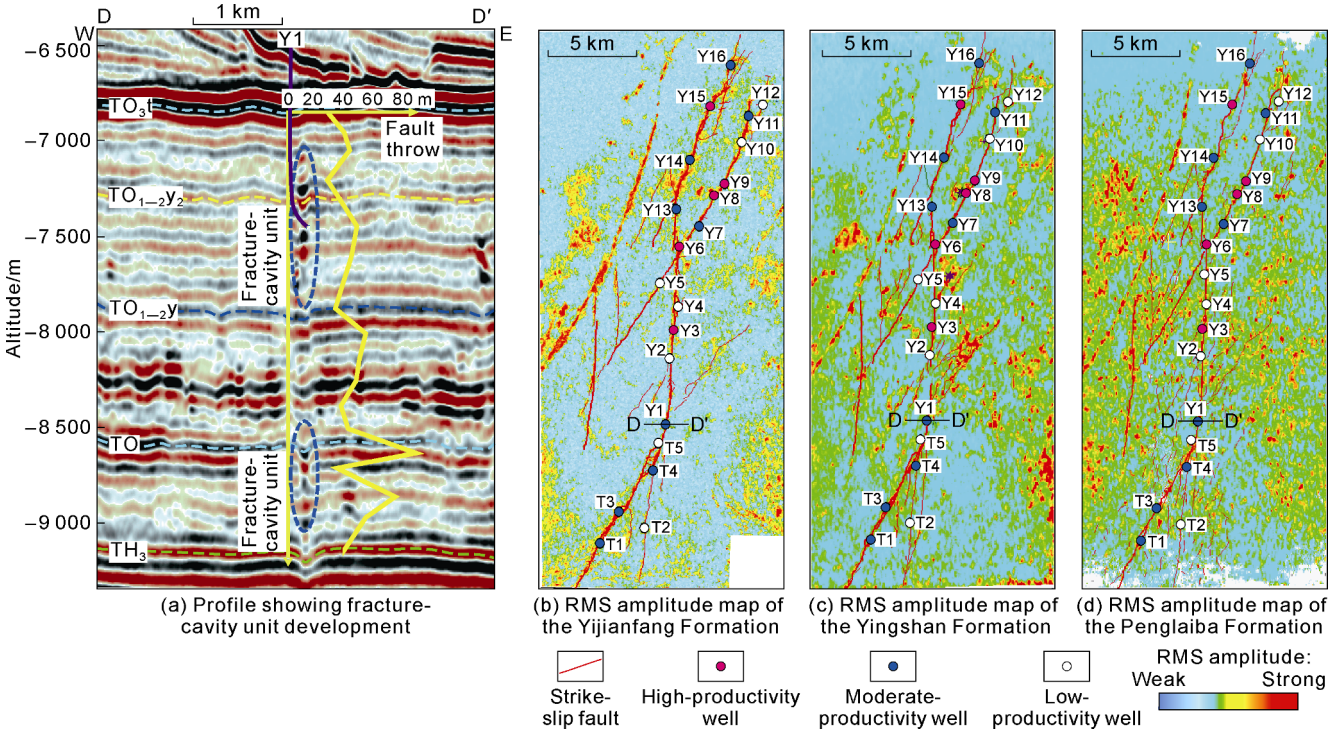

Fig. 4. Typical seismic profile and RMS amplitude maps of different formations showing Ordovician fracture-cavity units in the $F_1$19 fault zone (see profile location in Fig. 3a).

within the fault core but also widely distributed throughout the formation itself. Besides strike-slip faults, multiple phases of various karstification processes also play a critical role in the development of beaded reflections. The intraformational fracture-cavity units in the Lower Yingshan Formation and the Penglaiba Formation were formed through the modification by early fault activity and multi-phase karstification processes [14, 27–28].

The ultra-deep seismic profile across Well Y1 reveals that the strike-slip fault zone hosts fracture-cavity units in several Ordovician formations (Fig. 4a). Based on statistical analysis of vertical fault throws of strike-slip

faults, fracture-cavity units usually occur where the fault throw changes greatly. Root-mean-square (RMS) amplitude attribute maps of different formations reveal variations in the distribution of fracture-cavity units at various depths within the Ordovician. High-amplitude anomalies highlighted in red indicate the zones with fracture-cavity units developed. At the top of the Ordovician Yijianfang Formation, fracture-cavity units are primarily concentrated near the strike-slip fault zone (Fig. 4b). Within the Ordovician Yingshan Formation, fracture-cavity units are relatively developed inside the branch fault zones of the strike-slip fault system (Fig. 4c), while those in the Penglaiba Formation are chiefly distributed within the formations on both sides of the fault zone, where they form extensive fracture-cavity units due to the intraformational joints (Fig. 4d).

Integrated with seismic data, fracture-cavity units can be vertically classified into four types: top fractured, middle connected, deep terminated and intra-layer fractured. Due to the complex structures of the strike-slip fault zone, the principal displacement zone appears as a single fault strand at shallow depths in seismic profiles, and the associated fracture-cavity units display a top ruptured pattern. Strike-slip faults develop branch faults in both deep and middle parts, forming a flower-shaped structure, with the associated fracture-cavity units predominantly showing middle connected and deep terminated patterns. Widespread intra-layer fractured reservoirs occur in the Penglaiba Formation, resulting from interlayer joints and various karstification processes.

2.3. Structural model of ultra-deep strike-slip faults

By integrating field outcrop observations, seismic data, and ultra-deep drilling data, an improved vertical three-layer model of strike-slip faults has been established based on the pattern of fault core, fractured zone and primary rock (Fig. 5a). First, the fault core within the strike-slip fault zone contains fault clay, breccia, and fracture-cavity units. These units exhibit vertical heterogeneity in distribution. Due to the presence of fault clay and breccia, the fracture-cavity units are vertically compartmentalized and remain isolated from one another. Second, the fault band within the fractured zone contains the X-shaped shear joints and bedding-perpendicular tensile joints and bedding-parallel joints. Primary rock zone largely preserves the original lithological characteristics, with only minor fracture development. Within the complex strike-slip fault system in the ultra- deep strata of the Tarim Basin (Fig. 5b), multiple types of fracture-cavity units within multiple formations are identified. These units are concentrated within the flower-shaped structure, on both sides of the major fault zone and at the interfaces between strike-slip faults and formations, all showing significant vertical discontinuities.

3. Physical simulation experiment on vertical evolution process of strike-slip faults

Physical simulation was employed to validate the vertical evolution process of strike-slip faults and the distribution of associated fracture-cavity units. Moreover, particle image velocimetry (PIV) was used to monitor dynamic stress-strain changes in the fault zone and its surrounding fault blocks during experimentation. Based on these stress-strain variations, the rupture mechanisms of the fault and adjacent blocks, as well as the potential locations and distribution patterns of fracture-cavity units, were inferred.

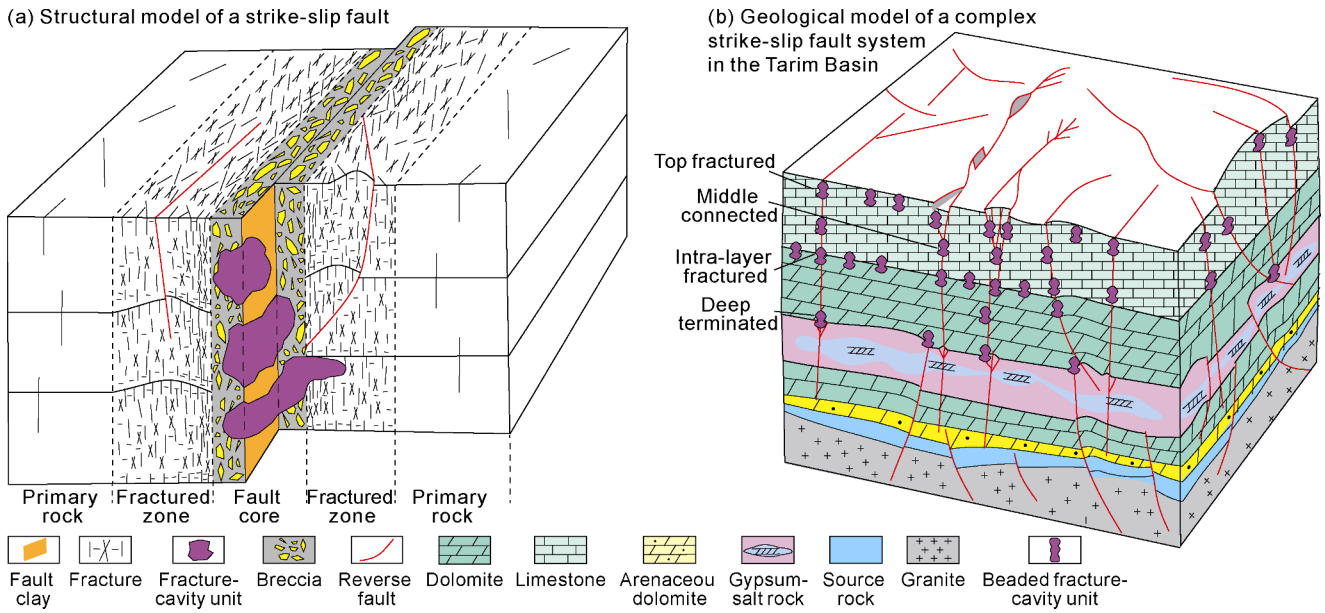

Fig. 5. Strike-slip fault model with fracture-cavity units.

3.1. Design

3.1.1. Protocol

Similar to previously established approaches, the physical simulation experimental method in this study uses wet quartz sand to simulate carbonate rock formations, and the relative displacement between two base plates to simulate the shear motion associated with strike-slip faulting [21]. Since the strike-slip faults were formed during the middle to late Caledonian period, contemporaneous with the deposition of the carbonate strata, and subsequently underwent deep burial, this experiment did not include an overburden layer. Compared with previous experimental processes, this study systematically observed the vertical formation and evolution of strike-slip faults, and recorded fault growth patterns as well as stress-strain variations, thus effectively documenting how the fault zone evolved.

The experiment was completed using the analog platform at the Physics Simulation Laboratory of China University of Petroleum (Beijing) at Karamay, Xinjiang. The analog platform primarily consists of three components: a main control console, a sandbox platform and a PIV monitoring system. The initial dimensions of the four experimental models ①–④ were 30 cm in length, 20 cm in width, and 4 cm in thickness. For observing the vertical rupture process, no boundary constraints were applied to the four sides of the model. Two rigid base plates measuring 0.5 cm × 20 cm × 60 cm were used as the substrate (Fig. 6). Driven by the motor, the two rigid base plates transfer motion to the overlying sand layer, inducing displacement. The shear motion between the plates simulates the relative slip of a strike-slip fault. The motion was halted after the fault had vertically evolved to maturity. The designed displacement of the base plates was relatively small, set at 2 cm. The motor, controlled by a computer, operated at a constant rate of 0.008 mm/s during the experiment. For experimental models ① and ②, a 4 cm thick layer of quartz sand was deposited on the two base plates without layered configuration. Dextral (or right-lateral) and sinistral (or left-lateral) strike-slip motions were applied to models ① and ②, respectively. In model ①, the left base plate was designated as the moving plate, while the right plate remained stationary. This configuration was reversed in model ②. For experimental models ③ and ④, a sequence of four 1-cm-thick quartz sand layers was constructed. Distinctive colored quartz sands with varying grain sizes were employed as marker layers between formations to enhance interlayer discrimination. The experimental procedures of models ① and ② were subsequently repeated (Fig. 6).

Under actual geological conditions, factors such as water content, and oil/gas content in formations may further complicate the internal structure of fault zones, but their influence on the vertical rupture and evolution processes of fault zones is not significant [18]. In the experiments, minor variations in the water content of the wet quartz sand, inconsistencies in sand layer construction, and differences in friction between the sand layers and the base plates across different models introduced slight errors into the results. These specific discrepancies are not discussed in this paper.

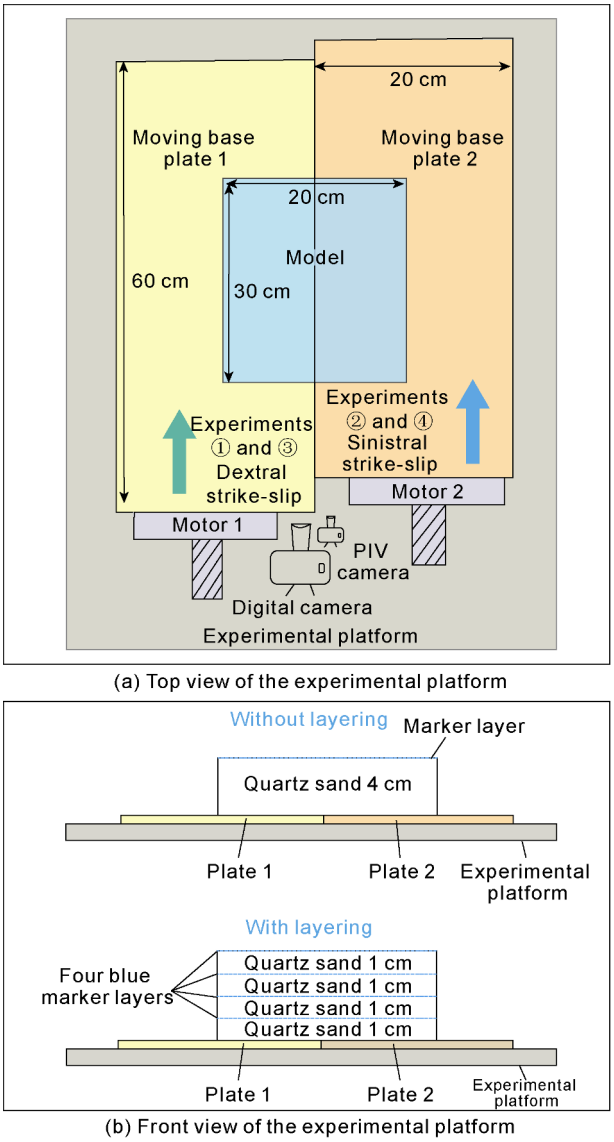

Fig. 6. Setup for physical simulation experiment on vertical growth of strike-slip faults.

3.1.2. Geological significance of the experiment

The varying experimental configurations, including motion directions (sinistral, dextral) and stratigraphic conditions (non-layered, layered) in the experiments is as are significant geologically in three aspects.

(1) Sinistral vs. dextral models: In the strike-slip fault systems of the Tarim Basin, some faults exhibit sinistral shear (e.g., the strike-slip fault system in the platform area of the Manjiaer Sag), while others demonstrate dex-

tral shear (e.g., the strike-slip fault system to the west of F_l15). Studying both sinistral and dextral shear models is crucial for identifying the influence of different strike-slip directions on fault geometry and growth patterns. These models simulate how regional tectonic stress fields differentially control the development, vertical growth, and connection of fault fracture-cavity units.

(2) Layered vs. non-layered models: The strata within the Tarim Basin exhibit distinct stratification characteristics. Differences in mechanical properties and lithology between layers significantly influence fault growth. The non-layered model simulates homogeneous stratigraphic conditions, revealing the growth process of strike-slip faults in a uniform lithological setting, thereby providing a reference for fundamental research. The layered model more closely approximates the actual geological conditions of the Tarim Basin, enabling the study of vertical fault growth patterns and fracture-cavity units' connectivity within layered media.

(3) Vertical growth mechanism research: By combining sinistral/dextral and layered/non-layered models, the experiments investigate how strike-slip faults with different motion directions grow vertically and affect various strata, and whether layered formations obstruct or direct the vertical growth of faults.

3.2. Experimental procedure

3.2.1. Structural physical simulation under non-layered conditions

According to the results of experimental model ① (Fig. 7), when the strike-slip displacement increases from 0 to 0.46 cm, no significant deformation or faulting is observed in the profile based on color photographs. As the strike-slip displacement is 0.52 cm, weak deformation emerges in both deep and shallow parts of the model, accompanied by minor fault formation. When the strike-slip displacement further increases to 0.61 cm, rupture occurs initially in the middle part of the model. At this stage, the faults are not yet interconnected, representing a stage of segmental rupture within the strike-slip system. As the strike-slip displacement increases from 0.61 cm to 0.75 cm, the faults progressively propagate and become interconnected vertically, marking the onset of the second evolutionary stage (vertical growth stage). With continued displacement beyond 0.75 cm, the fault zone becomes fully interconnected and expands in width, entering the third stage (extension stage). Throughout their growth, the faults tilt toward the active plate side due to its movement.

The accumulation process of finite shear strain reveals that, during the initial compression, when the strike-slip displacement reaches 0.46 cm, the finite shear strain intensifies (by approximately 4%) along the edges of the moving base plate and in the shallow part, but no

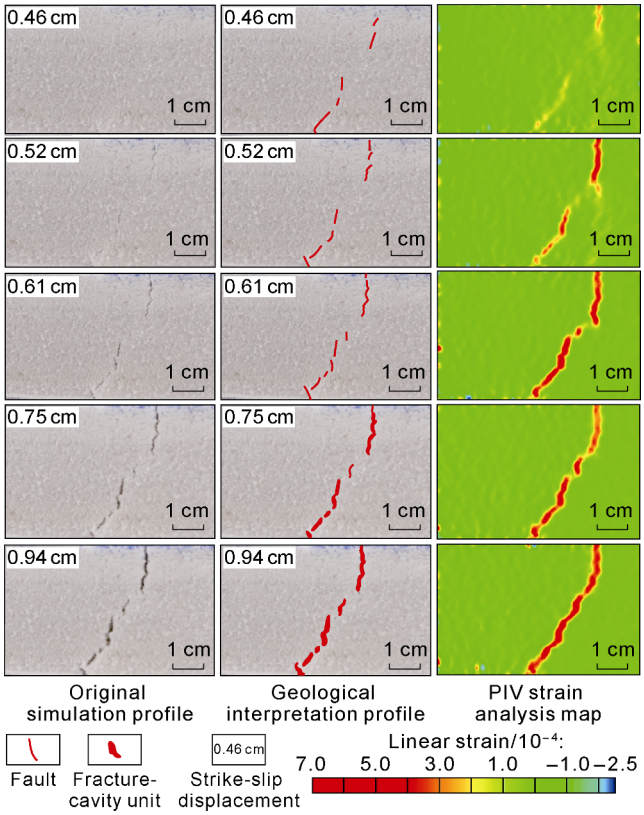

Fig. 7. Physical simulation of dextral strike-slip fault vertical growth under non-layered conditions (Experimental model ①).

significant faulting is observed in the model. As the strike-slip displacement increases to 0.52 cm, the finite shear strains in both deep and shallow parts gradually increase (by approximately 10%), leading to the development of distinct faults in strain-concentrated zones. With a further increase in strike-slip displacement to 0.75 cm, the zones with finite shear strain concentrated in the deep and shallow parts become interconnected, accompanied by a rise in strain intensity (by approximately 20%). This evolutionary process is consistent with the progression of fault growth.

The experiments document that, in the initial stage of shear motion, fault formation is not an instantaneous process. Initial minor faults emerge at different depths in deep, middle and shallow parts, with their formation exhibiting distinct time intervals. This temporal variation leads to differences in deformation patterns across various parts. Although this process occurs within a short time-frame, it indicates that strike-slip faults evolve in a segmental rupture-connection process over time.

Experimental model ② illustrates the growth process of a sinistral strike-slip fault (Fig. 8). In the initial stage, segmental rupture occurs. In contrast to model ①, the rupture in model ② first initiates in the middle part. Within a short time span, faults subsequently emerge in the deep and shallow parts of the model. PIV analysis of the profile indicates initial stress and strain concentrations first in the middle and basal sections, and intra-

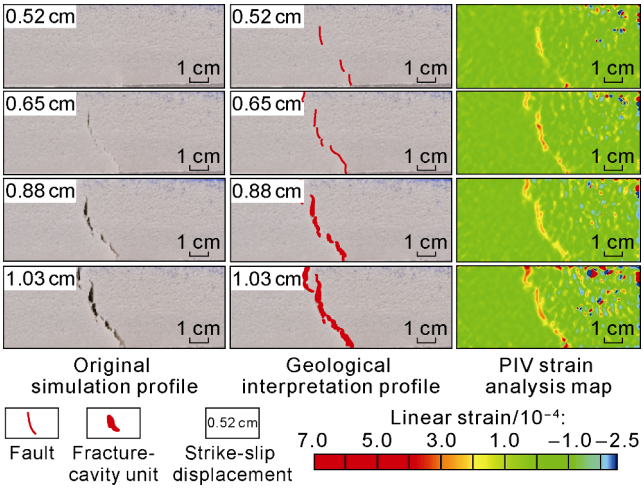

Fig. 8. Physical simulation of sinistral strike-slip fault vertical growth under non-layered conditions (Experiment model ②).

layer stress and strain concentration on the active plate side of the upper part. PIV technology can detect minute fractures that are difficult to discern with the naked eye. Heterogeneity is introduced into the shallow part due to the accidental incorporation of dry sand during the placement of colored marker layer at the top of the model. This heterogeneity leads to the creation of intra-layer micro-fissures, which diverts stress concentration away from the major fault zone in the shallow part. Instead, rupture occurs preferentially in the middle part of the model. In the fault growth and connection stage, the connection pattern is slightly different from the direct connection observed in experiment model ①. Specifically, lateral connection first forms between faults in the middle and shallow parts. Along with the lateral extension progressed, the lateral connection evolves into a vertically en échelon configuration, while fault cavities emerge within the fault zones in the middle and deep parts. The coexistence of vertically en échelon structures and fault cavities results in multiple segmented fracture-cavity units during subsequent lateral propagation. These units exhibit remarkable vertical compartmentalization with distinct soft-connection characteristics.

The finite shear strain accumulation process in experiment ② differs from that in experiment ①. Strain concentration initially occurs in the deep and middle parts of the model with an intensity of approximately 4%. When the strike-slip displacement is 0.56 cm, the strain concentration zones develop in a layered manner. As the displacement increases from 0.56 cm to 1.03 cm, the finite shear strain becomes most pronounced within fracture-cavity units of the fault zone, with an intensity of about 20%. Specifically, higher strain intensities are observed at locations corresponding to vertically en échelon structures and fault cavities, whereas lower strain intensities characterize the soft connection zones. This correlation suggests that areas with better fault connectivity exhibit stronger finite shear strain.

3.2.2. Structural physical simulation under layered conditions

For experimental models ③ and ④, blue dry quartz sand was incorporated as marker layers, while other experimental conditions are kept unchanged. In experiment ③, after segmental rupture occurs in the deep and shallow parts (Fig. 9), the fault zone undergoes two evolutionary stages: growth and connection, fault surface widening. This process shows high similarity with that in experiment ①. However, significant differences are observed in fault dip angles between shallow and deep parts in experiment ③, with shallow faults being near-vertical. Additionally, the dip angles of faults in the middle and deep parts are smaller than those in experiment ①. It is inferred that in the presence of multiple strata, differences at stratigraphic interfaces influence the connection between deep and shallow faults, leading to variations in rupture orientations across different layers. During the fault development process, a small fault (F2) is formed on the active plate side. This fault does not connect with the shallow faults. Under actual geological conditions, such deep faults that remain unconnected to shallow systems may serve as effective storage spaces for deep hydrocarbons, providing insights for the exploration of ultra-deep strike-slip fault reservoirs. The formation and evolution process of the fault in experiment ④ (Fig. 10) is similar to that in experiment ③. Both cases witness faults initially in the deep and shallow parts, which grow gradually until connection. Due to the influence of the marker layers, the faults exhibit bed-parallel development, with pronounced detachment structures observed at the base. This finding is highly consistent with field outcrop observations (Fig. 1), where prominent bed-parallel rupture also exists

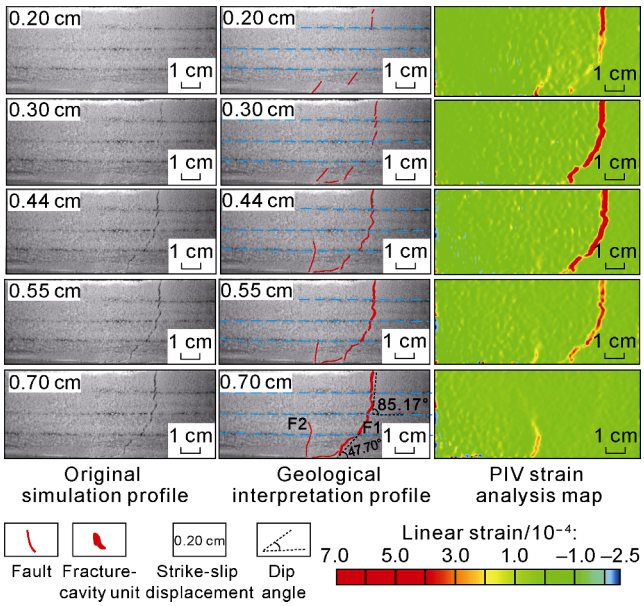

Fig 9. Physical simulation of dextral strike-slip fault vertical growth under layered conditions (Experiment model ③).

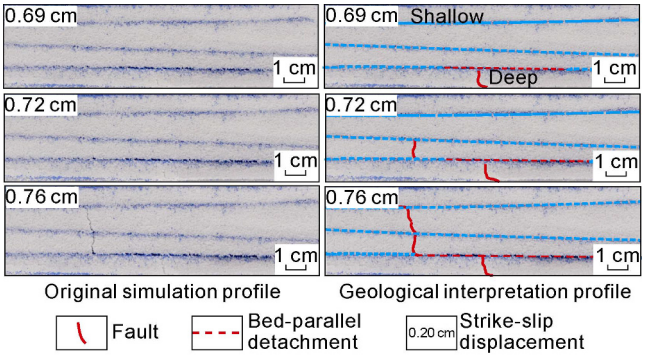

Fig. 10. Physical simulation of sinistral strike-slip fault vertical growth under layered conditions (Experiment model ④).

at the interface between Bed 25 and Bed 26. The difference in results of experiments ③ and ④ from those of experiments ① and ② is attributed to the use of quartz sand with varying grain sizes and water content as marker layers. These material variations alter the generation and transmission of stress and strain between different stratigraphic units, consequently modifying the vertical connection and evolutionary process of the strike-slip faults. In Experiment ④, significant deformation occurred in the model perpendicular to the cross-sectional plane, leading to suboptimal PIV results. Consequently, no effective analysis was conducted.

In Experiment ③, the finite shear strain accumulation process is initially manifested as vertical strain concentrations in the deep and shallow parts of the model. When the strike-slip displacement is 0.20 cm, the strain intensity in the shallow part (approximately 10%) exceeds that in the deep part, consistent with the observed wider faults in the shallow part on the profile. At a displacement of 0.44 cm, fault growth and connection occur, corresponding to the peak strain intensity (approximately 20%). As the displacement increases from 0.44 cm to 0.70 cm, deformation along the major fault is less pronounced, with gradual attenuation of strain intensity. Concurrently, F2 on the left progressively develops, demonstrating a systematic transfer of strain concentration from the major fault F1 to the small fault F2 in the profile. The PIV technique enabled the precise monitoring of differential stress and strain at different locations of the strike-slip fault over its developmental stages (Fig. 9).

3.3. Quantitative analysis of experimental results (addition of fracture-caivity units)

Given that Experiments ③ and ④ employed quartz sand of different particle sizes as marker layers, resulting in overly complex phenomena, they could not clearly illustrate the general patterns of the fracture-cavity system. Therefore, quantitative analysis was performed on faults in experiments ① and ② by measuring their width, length, and dip angle at different depths and evolutionary stages. This allows for comparison of vertical development characteristics across stages and depths. The results indicate that fault length and width increase linearly with displacement (Fig. 11). The initial faults occur at different positions, but the final faults are approximately twice of the initial faults in dimensions. Moreover, fault length and width exhibit significant variations at different depths, revealing the feature of differentiated growth across layers.

The experimental results also indicate that fault dip angles decrease with increasing depth. In the deep part of the

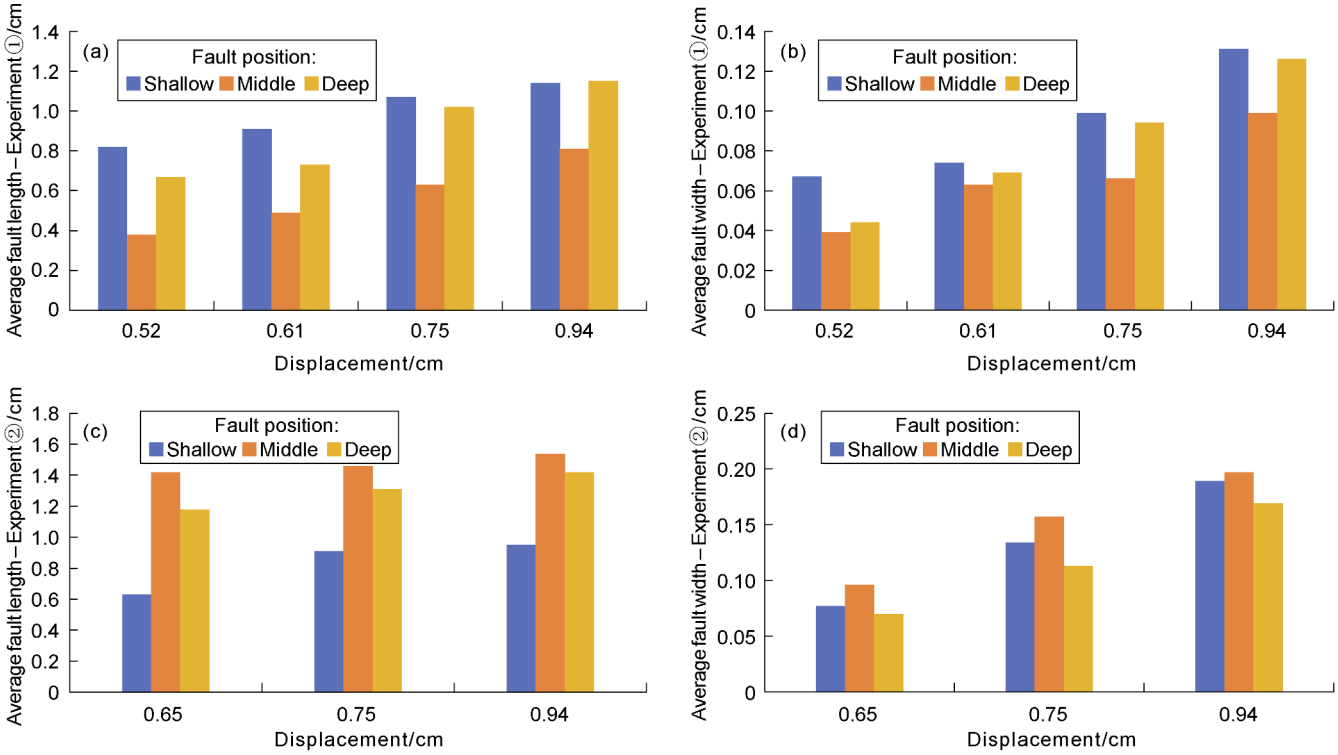

Fig. 11. Variations of fault length and width with displacement at varying depths in experiments ① and ②.

Table 1. Data analysis for structural physical simulation experiments on strike-slip fault vertical growth

Experiment	Displacement/cm	Shallow				Middle				Deep			
		Width/cm	Length/cm	L/W ratio	Dip angle/(°)	Width/cm	Length/cm	L/W ratio	Dip angle/(°)	Width/cm	Length/cm	L/W ratio	Dip angle/(°)
①	0.52	0.067	0.82	12.24	79.16	0.039	0.38	9.74	76.91	0.044	0.67	15.20	46.59
	0.61	0.074	0.91	12.30	81.96	0.063	0.49	7.78	81.04	0.069	0.73	10.57	47.51
	0.75	0.099	1.07	10.81	84.04	0.066	0.63	9.54	74.31	0.094	1.02	10.85	47.49
	0.94	0.131	1.14	8.70	81.97	0.099	0.81	8.18	78.61	0.126	1.15	9.12	53.28
②	0.65	0.077	0.63	8.18	86.84	0.096	1.42	14.79	63.6	0.070	1.18	16.86	48.78
	0.88	0.134	0.91	6.79	87.75	0.157	1.46	9.29	68.5	0.113	1.31	11.59	46.82
	1.03	0.189	0.95	5.03	87.40	0.197	1.54	7.82	68.2	0.169	1.42	8.40	49.30

model, the average dip angle is approximately 45°. In the middle part, the dip angle increases to 60°–70°. In the shallow part, the dip angle rises rapidly to near-vertical orientations, with most measurements exceeding 80° (Table 1).

Under actual geological conditions, there is no strict definition to distinguish between fractures and cavities in carbonate reservoirs. Morphologically, fractures are generally characterized by a length-to-width (L/W) ratio greater than 10 [29]. To describe the distribution patterns of fracture-cavity units, we define those with a L/W ratio less than 10 as fracture-cavity units. Analysis of the L/W ratios shows a general decreasing trend with increasing displacement in different parts, indicating a gradual expansion in the scale of fracture-cavity units (Table 1). In the connection and extension stage in experiments ① and ②, faults display the L/W ratios below 10, confirming the presence of fracture-cavity units. In the vertical growth stage, extensive fracture-cavity units appear in the middle part of Experiment ① and the middle and shallow parts in Experiment ②. Conversely, in the segmental rupture stage, most faults maintain the L/W ratios exceeding 10, with no fracture-cavity units observed on the profiles. These findings indicate that fracture-cavity units in strike-slip fault zones predominantly emerge during the middle to late stages of fault evolution.

3.4. Experimental conclusions

Based on structural physical simulation experiments of strike-slip fault vertical growth, a three-stage evolution model is established, comprising segmental rupture, vertical growth, and connection and extension (Fig. 12).

(1) Segmental rupture stage: The initial rupture of strike-slip fault exhibits a vertically layered pattern, with temporal variations across layers. In non-layered models, faults preferentially initiate from the deep and shallow parts (or the middle part) before propagating through the entire model. This may be attributed to the model heterogeneity (induced by, for instance, accidental sand mixing). In layered models, marker layers cause variations in stress distribution, leading to simultaneous rupture initiation in the deep and shallow parts. Additionally, bed-parallel detachment and dip angle variations occur along stratigraphic interfaces.

(2) Vertical growth stage: Faults created in the segmental rupture stage become gradually connected through

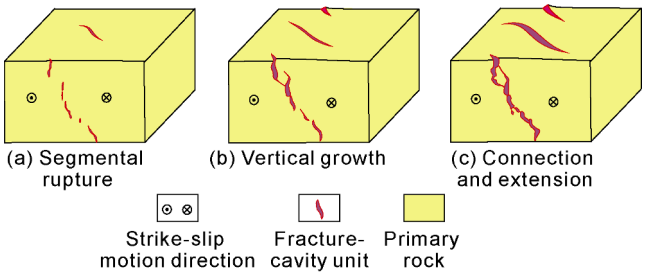

Fig. 12. Schematic model of strike-slip fault vertical growth.

vertical or lateral growth. In Experiment ①, faults are directly interconnected in vertical direction to form a continuous major fault zone. In Experiment ②, faults are connected laterally in vertically en échelon pattern, generating fault cavities within the middle and deep fault zones, with poor vertical connectivity. Under layered conditions, shallow faults exhibit steeper dips (near-vertical), while deep fault faults display decreased dips (45°–60°). Faults extend parallel to beds at marker layer interfaces, resulting in detachment or failure to connect secondary faults (e.g., F2). In this stage, fracture-cavity units begin developing, with the L/W ratio decreasing as the displacement increases (Table 2). Most fracture-cavity units (L/W ratio less than 10) are formed during mid-to-late stages, concentrating at the intersections of faults (e.g., en échelon cavities or major fault zones).

(3) Connection and extension stage: Following complete fault connection, lateral propagation dominates the evolution process, forming large-scale fracture-cavity systems. The width and length of the fault zone increase linearly. Fault cavities become vertically stacked and subsequently expand to form fracture-cavity units, enhancing overall cavern connectivity while maintaining vertical compartmentalization.

In summary, the variations in rock properties and cumulative displacement are the key controlling factors across all three evolutionary stages. At stratigraphic interfaces, differences in rock properties can lead to bed-parallel fault development, resulting in higher rupture intensity at these interfaces compared to other positions. Marker layers or heterogeneous layers alter stress transmission paths, influencing fault dip angles, connection patterns and bedding-parallel detachment. Fault width, length, and fracture-cavity dimensions all increase linearly with displacement, while decreasing length-to-width

ratios indicate the expansion of fracture-cavity units. The vertically segmental rupture and connection processes in strike-slip fault zones can form complex fracture-cavity networks, creating favorable storage spaces for deep hydrocarbon accumulation.

4. Characteristics and exploration potential of fracture-cavity units associated with ultra-deep strike-slip faults

Strike-slip faults with small to medium displacements are extensively distributed across the Tarim Basin. They universally exhibit a spatial structure defined by vertical stratification, planar segmentation, and multi-phase vertical stacking. The results of this study agree well with the characteristics of fractured-cavity reservoirs associated with ultra-deep strike-slip faults within the Fuman Oilfield of the Tarim Basin. This study establishes a vertical evolution model of strike-slip faults suitable for ultra-deep fault zones and clarifies the patterns of fracture-cavity units. These results provide valuable references for investigation of strike-slip faults in other basins [30–32].

The F_I19 strike-slip fault zone in the Fuman Oilfield exhibits significant development of fracture-cavity units. In profile view (Fig. 4a), these units present a beaded distribution perpendicular to the strike-slip fault. In planar view (Fig. 4b–4d), they appear in a spotted pattern or in a banded pattern along the strike-slip fault zone. The extensive fracture-cavity units provide substantial storage space for hydrocarbons, indicating a considerable potential for petroleum exploration.

The fractured-cavity reservoirs controlled by the F_I19 strike-slip fault zone can be classified into three types: (1) flower-shaped fractured reservoirs encountered in wells Y9 and Y8; (2) deep and large fault reservoirs penetrated by well Y6; and (3) staggered overlapping reservoirs drilled by well Y5 (Fig. 13). The flower-shaped fractured reservoirs and large and deep fault reservoirs demonstrate superior fault connectivity, creating larger storage space for greater hydrocarbon accumulation, thus holding larger reservoirs and exploration potential. In contrast, the staggered overlapping reservoirs exhibit relatively poorer connectivity, corresponding to constrained storage space, thus implying smaller reservoir size and limited exploration potential, compared to the first two types. Production data substantiate this distinction (Table 2): wells Y9 and Y8 (flower-shaped fractured-cavity reservoirs) and well Y6 (large and deep fault reservoirs) all represent high-productivity wells, demonstrating pressure-drop production rates of 6 246.15, 7 287.74, and 5 218.85 t/MPa, respectively.

It is indicated that ultra-deep formations still possess conditions conducive to the development of fracture-cavity units. The deep units are typically closer to hydrocarbon source rocks and can form effective reservoirs

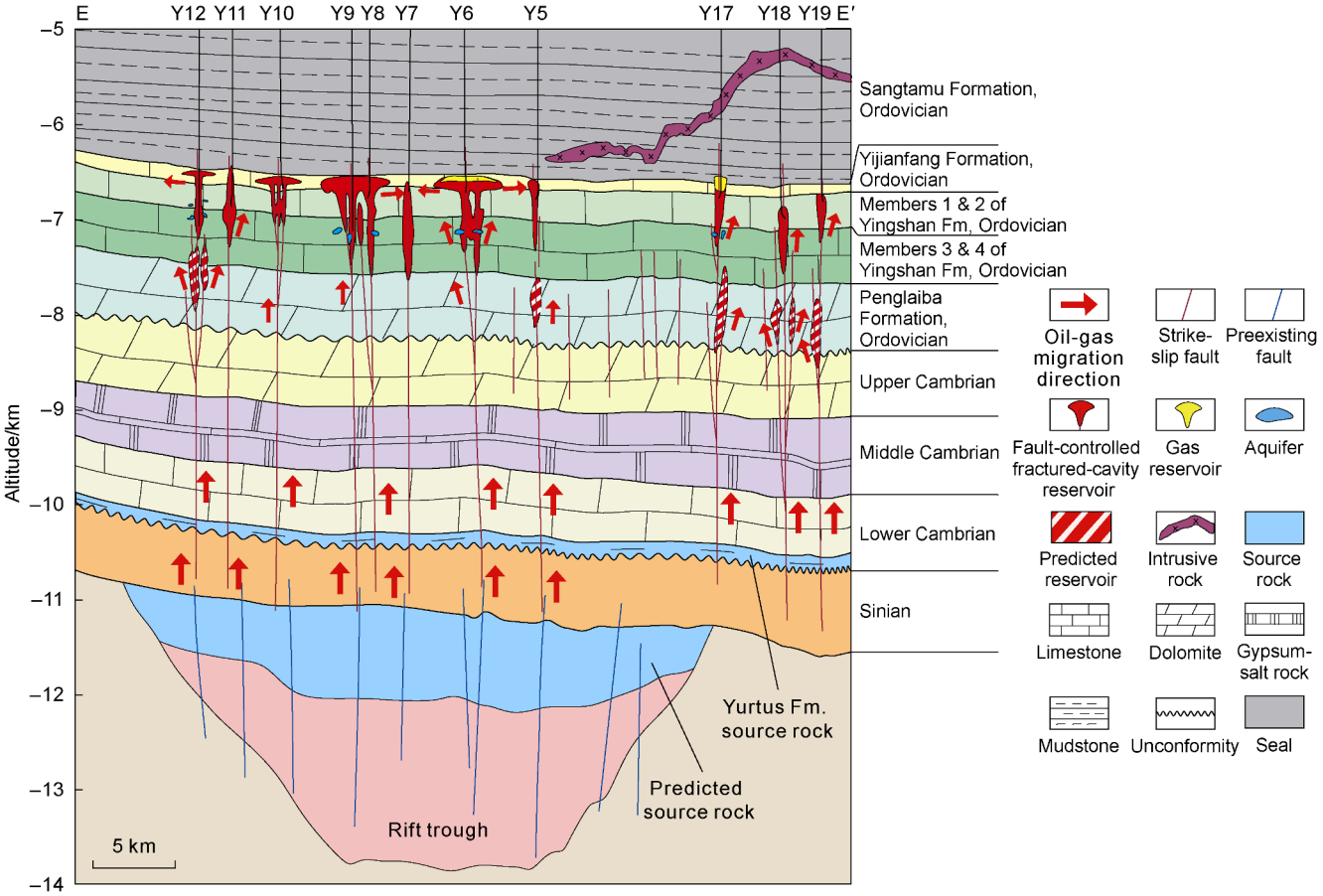

Fig. 13. Reservoir profile of the F_I19 strike-slip fault zone (profile location shown in Fig. 3a).

Table 2. Statistical data of typical wells in the F_I19 strike-slip fault zone, Fuman Oilfield

Well	Average daily liquid production/t	Average daily oil production/t	Average daily gas production/m^3	Water cut/%	GOR/ ($m^3 \cdot t^{-1}$)	Pressure-drop production/ ($t \cdot MPa^{-1}$)	Well type	Productivity level
Y17	47.50	46.67	23 542	1.75	504.48	270.43	Commercial oil well	Low-productivity
Y12	44.27	43.07	15 801	2.72	366.89	98.76	Commercial oil well	Low-productivity
Y11	48.84	48.27	16 241	1.18	336.47	541.92	Commercial oil well	Medium-productivity
Y10	64.27	63.49	21 588	1.21	340.01	225.32	Commercial oil well	Low-productivity
Y9	84.00	83.26	21 876	0.88	262.74	6 246.15	Commercial oil well	High-productivity
Y8	91.51	90.33	29 309	1.29	324.47	7 287.74	Commercial oil well	High-productivity
Y7	94.81	93.86	34 216	1.00	364.54	94.81	Commercial oil well	Low-productivity
Y6	88.01	86.67	43 522	1.52	502.15	5 218.85	Commercial oil well	High-productivity

Note: High-productivity wells are defined by a pressure-drop production rate exceeding 2 000 t/MPa; medium-productivity wells correspond to a pressure-drop production rate of 500–2 000 t/MPa; low-productivity wells are characterized by pressure-drop production rates below 500 t/MPa.

when adequate sealing conditions exist. Current exploration efforts have primarily focused on members 1–2 of the Yingshan Formation, while the deeper members 3–4 of the Yingshan Formation and the Penglaiba Formation also contain beaded fracture-cavities and intralayer faults. These deeper zones show significant exploration potential and represent key targets for future exploration.

5. Conclusions

The strike-slip fault zone of ultra-deep Tarim Basin presents a three-layer structure, consisting of fault core, fracture zone and primary rock. The fault core vertically includes fracture-cavity unit, fault clay and breccia.

The strike-slip faults have evolved vertically in three stages: segmental rupture, vertical growth, and connection and extension. In the segmental rupture stage, multiple segmented rupture zones develop vertically within the strata. Due to lithological differences, the timing of rupture initiation differs between deep and shallow parts. In the vertical growth stage, the faults created in the rupture stage become connected vertically or laterally to form a major fault zone, accompanied by the generation of fault cavities. Moreover, detachment occurs along stratigraphic interfaces. In the connection and extension stage, following complete fault connection, faults propagate laterally, giving rise to fracture-cavity units. Experimental data indicate that the fault width, length and fracture-cavity scale increase linearly with the displacement, while a decrease in the length-to-width ratio reflects the enlargement of fracture-cavity dimensions.

Fracture-cavity units in ultra-deep formations can be classified into four types: top fractured (shallow vertical faults), middle connected (branch faults in flower-shaped structures), deep terminated (non-connected vertical portions by faults), and intra-layer fractured (intraformational joints and karstification superimposed).

The flower-shaped fractured and large and deep fault reservoirs are larger in size with superior connectivity and large reservoir space, suggesting a significant exploration potential. The staggered overlapping reservoirs show poor connectivity that impedes hydrocarbon migration, corresponding to high exploration risk and necessitating further study of migration pathways.

References

[1] WANG Qinghua. Differential deformation and evolution characteristics of the no.17 strike-slip fault zone in the Tarim Basin. Geoscience, 2023, 37(5): 1136–1145.

[2] ZHANG Yintao, CHEN Shi, LIU Qiang, et al. Development characteristics and evolution model of FI19 fault in Fuman Oilfield, Tarim Basin. Geoscience, 2023, 37(2): 283–295.

[3] LIU Qiang, ZHANG Yintao, CHEN Shi, et al. Development and evolution characteristics of strike-slip faults in Tarim Basin and its geological significance: A case study of F_I17 fault in Fuman Oilfield. Geoscience, 2023, 37(5): 1123–1135.

[4] ZHANG Shuichang, WANG Huajian, SU Jin, et al. Control of earth system evolution on the formation and enrichment of marine ultra-deep petroleum in China. Petroleum Exploration and Development, 2024, 51(4): 759–773.

[5] WANG Qinghua, YANG Haijun, WANG Rujun, et al. Discovery and exploration technology of fault-controlled large oil and gas fields of ultra-deep formation in strike slip fault zone in Tarim Basin. China Petroleum Exploration, 2021, 26(4): 58–71.

[6] TIAN Jun, YANG Haijun, ZHU Yongfeng, et al. Geological conditions for hydrocarbon accumulation and key technologies for exploration and development in Fuman Oilfield, Tarim Basin. Acta Petrolei Sinica, 2021, 42(8): 971–985.

[7] WANG Qinghua. Origin of gas condensate reservoir in

Fuman Oilfield, Tarim Basin, NW China. Petroleum Exploration and Development, 2023, 50(6): 1128–1139.

[8] NENG Yuan, WU Guanghui, HUANG Shaoying, et al. Formation stage and controlling factors of the paleo-uplifts in the Tarim Basin: A further discussion. Natural Gas Industry, 2016, 36(4): 27–34.

[9] WANG Tieguan, SONG Daofu, LI Meijun, et al. Natural gas source and deep gas exploration potential of the Ordovician Yingshan Formation in the Shunnan-Gucheng region, Tarim Basin. Oil & Gas Geology, 2014, 35(6): 753–762.

[10] WANG Rujun, WANG Xuan, DENG Xingliang, et al. Control effect of strike-slip faults on carbonate reservoirs and hydrocarbon accumulation: A case study of the northern depression in the Tarim Basin. Natural Gas Industry, 2021, 41(3): 10–20.

[11] DENG Shang, LI Huili, HAN Jun, et al. Characteristics of the central segment of Shunbei 5 strike-slip fault zone in Tarim Basin and its geological significance. Oil & Gas Geology, 2019, 40(5): 990–998.

[12] DENG Shang, LI Huili, ZHANG Zhongpei, et al. Characteristics of differential activities in major strike-slip fault zones and their control on hydrocarbon enrichment in Shunbei area and its surroundings, Tarim Basin. Oil & Gas Geology, 2018, 39(5): 878–888.

[13] NENG Yuan, YANG Haijun, DENG Xingliang. Structural patterns of fault broken zones in carbonate rocks and their influences on petroleum accumulation in Tazhong Paleo-uplift, Tarim Basin, NW China. Petroleum Exploration and Development, 2018, 45(1): 40–50.

[14] QI Lixin. Oil and gas breakthrough in ultra-deep Ordovician carbonate formations in Shuntuoguole uplift, Tarim Basin. China Petroleum Exploration, 2016, 21(3): 38–51.

[15] KUANG Anpeng, YU Yixin, ZHU Xiuxiang, et al. Deformation and activity characteristics of the No. 11 strike-slip fault zone in the Shunbei area, Tarim Basin. Geoscience, 2021, 35(6): 1809–1817.

[16] WU Guanghui, MA Bingshan, HAN Jianfa, et al. Origin and growth mechanisms of strike-slip faults in the central Tarim cratonic basin, NW China. Petroleum Exploration and Development, 2021, 48(3): 510–520.

[17] WANG Z Y, GAO Z Q, FAN T L, et al. Structural characterization and hydrocarbon prediction for the SB5M strike-slip fault zone in the Shuntuo Low Uplift, Tarim Basin. Marine and Petroleum Geology, 2020, 117: 104418.

[18] DOOLEY T P, SCHREURS G. Analogue modelling of intraplate strike-slip tectonics: A review and new experimental results. Tectonophysics, 2012, 574/575: 1–71.

[19] CLOOS H. Experimente zur inneren tektonik. Zentralblatt für Mineralogie, Geologieund Paläontologie Abhandlungen B, 1928(12): 609–621.

[20] NAYLOR M A, MANDL G, SUPESTEIJN C H K. Fault geometries in basement-induced wrench faulting under different initial stress states. Journal of Structural Geology, 1986, 8(7): 737–752.

[21] XIAO Yang, WU Guanghui, LEI Yongliang, et al. Analogue modeling of through-going process and development pattern of strike-slip fault zone. Petroleum Exploration and Development, 2017, 44(3): 340–348.

[22] NENG Y, LI Y, QI J F, et al. Deformation styles and multistage evolution history of a large intraplate strike-slip fault system in a Paleozoic superimposed basin: A case study from the Tarim Basin, NW China. Frontiers in Earth Science, 2022, 10: 837354.

[23] HAN X Y, DENG S, TANG L J, et al. Geometry, kinematics and displacement characteristics of strike-slip faults in the northern slope of Tazhong uplift in Tarim Basin: A study based on 3D seismic data. Marine and Petroleum Geology, 2017, 88: 410–427.

[24] LI M J, WANG T G, CHEN J F, et al. Paleo-heat flow evolution of the Tabei Uplift in Tarim Basin, northwest China. Journal of Asian Earth Sciences, 2010, 37(1): 52–66.

[25] HOU Shaoyong, DUAN Peize, HE Qingqing, et al. Study on the favorable reservoir area of strike-slip fault zone of ultra-deep carbonate reservoir in Fuman Oilfield. Offshore Oil, 2023, 43(1): 10–15.

[26] CHEN S, ZHANG Y T, XIE Z, et al. Multi-stages of Paleozoic deformation of the fault system in the Tazhong Uplift, Tarim Basin, NW China: Implications for hydrocarbon accumulation. Journal of Asian Earth Sciences, 2024, 265: 106086.

[27] WANG Qinghua, YANG Haijun, ZHANG Yintao, et al. Great discovery and its significance in the Ordovician in Well Fudong 1 in Fuman Oilfield, Tarim Basin. China Petroleum Exploration, 2023, 28(1): 47–58.

[28] NI Xinfeng, SHEN Anjiang, QIAO Zhanfeng, et al. Genesis and exploration enlightenment of Ordovician fracture-vuggy carbonate karst reservoirs in Tarim Basin. Lithologic Reservoirs, 2023, 35(2): 144–158.

[29] WANG Xiaoyao, ZENG Lianbo, WEI Hehua, et al. Research progress of the fractured-vuggy reservoir zones in carbonate reservoir. Advances in Earth Science, 2018, 33(8): 818–832.

[30] MA Bingshan, LIANG Han, WU Guanghui, et al. Formation and evolution of the strike-slip faults in the central Sichuan Basin, SW China. Petroleum Exploration and Development, 2023, 50(2): 333–345.

[31] HE Dengfa. Multi-cycle superimposed sedimentary basins in China: Formation, evolution, geologic framework and hydro-carbon occurrence. Earth Science Frontiers, 2022, 29(6): 24–59.

[32] TANG Daqing, CHEN Honghan, GENG Feng, et al. Characteristics of intraplate small-displacement strike-slip faults: A case study of Tarim, Sichuan and Ordos basins. Earth Science, 2023, 48(6): 2067–2086.